Supporting Information

Li et al. 10.1073/pnas.1219420110

SI Symmetry Analysis of the Optical Selectivity

Here, we show the derivation of Eq. **6** in the text. We are concerned with the optical selectivity between Bloch states, n and n', both at crystal momentum $\mathbf{k}$ and of spin s. The interband matrix element $P_{\pm} = \langle n'\mathbf{k}, s|p_x \pm ip_y|n\mathbf{k}, s\rangle$ is given in the text below Eq. **5**. The selectivity may be derived by inspecting the effects of threefold roation, $\hat{C}_3$, on the matrix element. We insert the operator $\hat{C}_3$ into $P_{\pm}$:

$$P_{\pm} = \left\langle n'\mathbf{k}, s|\hat{C}_3^{-1}\hat{C}_3(p_x \pm ip_y)\hat{C}_3^{-1}\hat{C}_3|n\mathbf{k}, s\right\rangle. \quad [S1]$$

When we operate $\hat{C}_3$ on an eigenstate at $\mathbf{k}$, we have $\hat{C}_3|n\mathbf{k}, s\rangle = \exp(i\varphi_{n\mathbf{k}})|n\mathbf{k}, s\rangle$, where $\varphi_{n\mathbf{k}} = l_{n\mathbf{k}}2\pi/3$. Under $\hat{C}_3$, $(p_x + ip_y)$ transforms as

$$\hat{C}_3(p_x \pm ip_y)\hat{C}_3^{-1} = \exp\left(\mp\frac{2\pi}{3}\right)(p_x \pm ip_y). \quad [S2]$$

It follows, then,

$$P_{\pm} = e^{\left[-i\left(l_{n'\mathbf{k}} - l_{n\mathbf{k}} \pm 1\right)\frac{2\pi}{3}\right]}P_{\pm}. \quad [S3]$$

When $\text{modulo}(l_{n\mathbf{k}} - l_{n'\mathbf{k}}, 3) = +1$ we have $P_+ = P_+$ and $P_- = e^{i4\pi/3}P_-$. It follows $P_- = 0$. According to Eq. **5**, $\eta^{(s)}(\mathbf{k}) = 1$, corresponding to the absorption of the left-polarized light. In a similar manner, $\text{modulo}(l_{n\mathbf{k}} - l_{n'\mathbf{k}}, 3) = -1$ means $P_+ = 0$ and $\eta^{(s)}(\mathbf{k}) = -1$, corresponding to the absorption of the right-polarized light.

SI Bilayer Manganese Chalcogenophosphates

Bilayer or few-layer $MnPX_3$ also may have interesting spin and valley physics, similar to the spontaneous symmetry-broken few-layer graphene system (1). To consider different kinds of stacking and magnetic order of bilayer $MnPX_3$(X = S, Se), van der Waals corrections within generalized gradient approximation are included by the optB86b-vdwDF method in our calculation (2, 3). Further details of the calculations may be found in *Methods*. For antiferromagnetic bilayer $MnPX_3$ composed of intralayer antiferromagnetic monolayer, we calculate three kinds of stacking order, namely AA, AB and bulk-like (BL). The AA and AB stacking are similar to bilayer graphene (4, 5), and the BL stacking is obtained by taking two neighboring layers out of monoclinic bulk $MnPX_3$ (6). Moreover, taking interlayer antiferromagnetic or ferromagnetic order into account, there are six possible geometric and magnetic structures. The energy of antiferromagnetic monolayer $MnPX_3$ is used as a reference (set to zero), and all energies are given in electronvolts per $(MnPX_3)_2$. As shown in Table S1, two AA stackings, with interlayer ferromagnetic and antiferromagnetic order, respectively, are nearly degenerate in energy and the most stable bilayer structures. Compared with ferromagnetic (both intralayer and interlayer ferromagnetic orders) and nonmagnetic states in Table S2, we find that the antiferromagnetic order indeed is the most stable, as bulk and monolayer $MnPX_3$. Then, we focus on the two antiferromagnetic bilayers with AA stacking in the subsequent calculations.

The band structures of bilayer $MnPX_3$ with intralayer antiferromagnetic order are shown in Fig. S1. As in the monolayer case, spin degeneracy remains everywhere in the momentum space. All structures show direct band gaps at $\mathbf{K}_{\pm}$, similar to monolayer $MnPX_3$. Bilayer $MnPS_3$ and $MnPSe_3$ with interlayer ferromagnetic coupling have direct band gaps of 2.35 and 1.67 eV, respectively. The antiferromagnetically coupled bilayer $MnPS_3$ and $MnPSe_3$ have direct band gaps of 2.38 and 1.71 eV, respectively. These gaps are smaller than that of monolayer $MnPX_3$, and again fall within the optical range. We also compute the momentum-resolved spin-dependent degree of circular polarization of bilayer $MnPX_3$ (Fig. S2). The $s \cdot \tau$ circular dichroism is present in ferromagnetically coupled bilayers, with no inversion center in the magnetic space group. The chiral optical selection rule is absent in the case of antiferromagnetic interlayer coupling, as expected.

1. Zhang F, Jung J, Fiete GA, Niu Q, MacDonald AH (2011) Spontaneous quantum Hall states in chirally stacked few-layer graphene systems. *Phys Rev Lett* 106(15):156801.
2. Klimeš J, Bowler DR, Michaelides A (2010) Chemical accuracy for the van der Waals density functional. *J Phys Condens Matter* 22(2):022201.
3. Klimeš J, Bowler DR, Michaelides A (2011) Van der Waals density functionals applied to solids. *Phys Rev B* 83:195131.
4. Ho JH, Lu CL, Hwang CC, Chang CP, Lin MF (2006) Coulomb excitations in AA- and AB-stacked bilayer graphites. *Phys Rev B* 74:085406.
5. Liu Z, Suenaga K, Harris PJF, Iijima S (2009) Open and closed edges of graphene layers. *Phys Rev Lett* 102(1):015501.
6. Ressouche E, et al. (2010) Magnetoelectric $MnPS_3$ as a candidate for ferrotoroidicity. *Phys Rev B* 82:100408.

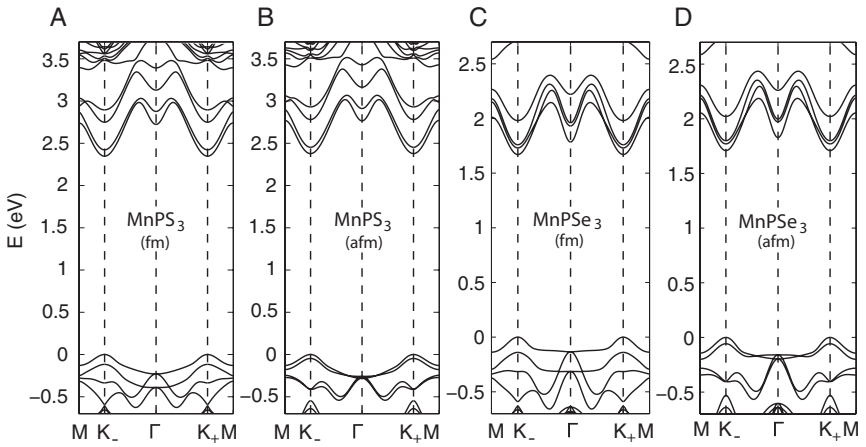

Fig. S1. Band structures of intralayer antiferromagnetic bilayer $MnPX_3$ with AA stacking near the band gaps. Ferromagnetically (*A*) and antiferromagnetically (*B*) coupled bilayer $MnPS_3$, and ferromagnetically (*C*) and antiferromagnetically (*D*) coupled bilayer $MnPSe_3$.

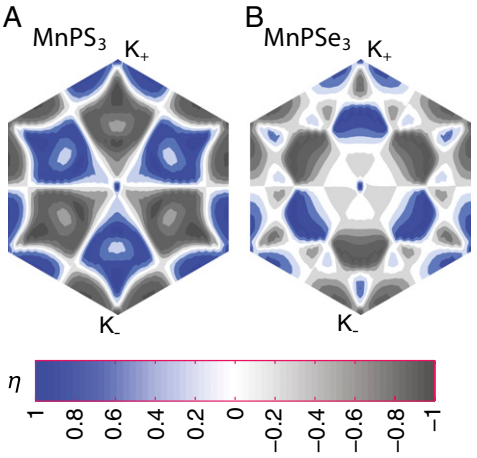

Fig. S2. Degrees of circular polarization of ferromagnetically coupled bilayer (*A*) $MnPS3_3$ and (*B*) $MnPSe_3$ computed using the linear response approach. The values of only one spin are presented, as in our calculations, the other spin takes values equal in magnitude but with opposite signs over the Brillouin zone.

Table S1. Energies of bilayer $MnPX_3$ with intralayer antiferromagnetism

	Energy (eV)					
	AA-afm	AA-fm	AB-afm	AB-fm	BL-afm	BL-fm
$MnPS_3$	−1.034	−1.022	−0.986	−0.982	−0.945	−0.945
$MnPSe_3$	−1.147	−1.146	−1.129	−1.121	−1.083	−1.086

afm, antiferromagnetic; fm, ferromagnetic.

Table S2. Energies of ferromagnetic and nonmagnetic bilayer $MnPX_3$

	Energy (eV)					
	AA-fm	AA-nm	AB-fm	AB-nm	BL-fm	BL-nm
$MnPS_3$	−0.964	5.208	−0.907	5.112	−0.888	5.118
$MnPSe_3$	−1.102	5.103	−1.089	5.188	−1.052	5.239

fm, ferromagnetic; nm, nonmagnetic.